The Journal of Physical Chemistry B

 VOLUME 103, NUMBER 32, AUGUST 12, 1999

LETTERS

Multiple-Exponential Electron Injection in $Ru(dcbpy)_2(SCN)_2$ Sensitized ZnO Nanocrystalline Thin Films

John B. Asbury, YongQiang Wang, and Tianquan Lian*

Department of Chemistry, Emory University, Atlanta, Georgia 30322

Received: May 19, 1999; In Final Form: June 28, 1999

We have studied the electron injection dynamics of $Ru(dcbpy)_2(SCN)_2$ sensitized ZnO nanocrystalline thin films by femtosecond mid-IR absorption spectroscopy. Upon 400 nm excitation of the sensitizer, nonexponential electron injection kinetics from the sensitizer MLCT excited state to ZnO were observed by probing the absorption of injected electrons in the 2000 to 1900 cm^{-1} region on the <1 ns time scale. A three-exponential fit to the data yields the following rise time constants and amplitudes (in parentheses): < 1ps (18%), 42ps (46%), and 450ps (36%). For films with increasing coverage of sensitizer molecules (optical density at 500 nm of 0.7, 2.3, 2.6), similar electron injection times were observed, while the injection yield decreases. This result suggests that aggregation or multilayer formation of sensitizer molecules reduces the quantum yield of electron injection to ZnO on the <1 ns time scale, and the observed multiexponential injection kinetics are attributed to the distribution of injection rates from the first monolayer of sensitizers. Possible reasons for the nonexponential injection are discussed. The injection dynamics are also compared with the very different injection dynamics observed for the same sensitizer on TiO_2.

Introduction

A new approach to building efficient, cost-effective solar cells has been to use transparent nanocrystalline films made of wide band gap semiconductors spectrally sensitized with a surface adsorbed dye[1]. An example of an efficient combination of semiconductor and sensitizer is TiO_2 nanocrystalline thin film sensitized with the sensitizer $Ru(II)(dcbpy)_2(SCN)_2$ (dcbpy = 2,2′-bipyridyl-4,4′-dicarboxylato)[2] referred to as Ru N3 from this point forward. This combination has been shown to operate with about 10% efficiency at converting solar power into electrical power.[2] Many studies of Ru N3 on TiO_2 have yielded detailed knowledge of the photophysics of the sensitizer,[2−4] how the sensitizer interacts with the semiconductor surface,[5−7] how electron injection occurs,[3,8−12] and the morphology and electron transport properties of the semiconductor thin film.[13−19] Forward electron injection from Ru N3 to TiO_2 was found to occur on the <100 fs time scale,[3,8−12] while the back electron transfer occurs on the microsecond to millisecond time scale.[10,20] The combined ultrafast electron injection and slow recombination ensures a high photon-to-current conversion efficiency.

Solar cells made from Ru N3 on ZnO have been found to operate only with 0.5−2% overall solar to electric power conversion efficiency,[21−23] even though bulk ZnO and TiO_2 have almost the same valence and conduction band energies.[1] The reason for the low conversion efficiency is so far unclear.[21,22] Previously, we directly determined the rate of electron transfer from several sensitizers to the semiconductor by measuring the rise of the mid-IR absorption signal due to electrons in the conduction band.[3,8,9,24,25] We have recently studied the injection time of Ru N3 sensitized ZnO nanocrystalline thin films with the same technique. In contrast to the previously observed <100 fs electron injection time in Ru N3 sensitized TiO_2 thin

* To whom correspondence should be addressed: e-mail, tlian@emory.edu.

10.1021/jp991625q CCC: $18.00
Published on Web 07/23/1999

films,[3,8−12] the electron injection process in Ru N3 sensitized ZnO thin films is much slower and is distinctly non-single-exponential.

In addition to its relevance to solar cell performance, the sensitized ZnO system also serves as an interesting model to study interfacial electron transfer. Ultrafast subpicosecond electron injection times in dye sensitized TiO_2 nanoparticle colloids and thin films have been observed by many groups in recent years.[3,8−12,24,25] However, the detailed mechanism for the ultrafast injection has not been clearly established. In the strong coupling limit, the electron injection can be a barrierless adiabatic process with injection times on the <100 fs time scale.[26] Ultrafast electron injection prior to vibrational relaxation has been proposed to describe the injection process in the Ru N3 sensitized TiO_2 thin films.[11] The observed slower electron injection time in the ZnO film would suggest a nonadiabatic ET process with weak electronic coupling. In this case, the rate of electron transfer is dependent on the electronic coupling element, driving force, density of acceptor states, and reorganization energy.[26] In addition, unlike TiO_2, small ZnO nanoparticles that show a quantum confinement effect can be prepared,[27−30] and the effect of quantum confinement on ET dynamics can be investigated. In this paper, we report the nonexponential electron injection dynamics on Ru N3 sensitized ZnO thin film. We discuss the possible reasons for the observed nonexponential injection dynamics and the differences compared to the Ru N3 sensitized TiO_2 thin films.

Methods

Femtosecond IR Spectrometer. The femtosecond infrared spectrometer used for this study is based on an amplified femtosecond Ti:sapphire laser system from Clark-MXR (1 kHz repetition rate at 800 nm, 100 fs, 900 μJ/pulse), and nonlinear frequency mixing techniques. The details of this set up have been described elsewhere.[24] Briefly, the samples were probed with a mid-IR pulse generated by combining the signal and idler output of an IR optical parametric amplifier in a $AgGaS_2$ crystal. The mid-IR was then dispersed in a monochromator, and 2−3 cm^{-1} slices of the spectrum were measured by a pair of HgCdTe detectors. Differential absorbance measurements were made with adjacent pulses by blocking every other pump pulse with a synchronized chopper. Moving film samples were pumped at 400 nm, and the subsequent absorbance change in the 1900 to 2000 cm^{-1} region was measured. The pump energy was 3 mJ, and the diameter of the pump and probe beams at the sample were 550 and 250 μm, respectively. The zero delay time and instrument response for the 400 nm pump, mid-IR probe experiments were determined in a thin silicon wafer. The typical instrument response function measured is well presented by a Gaussian function with a fwhm of about 190 fs.

Sample Preparation. The ZnO nanoparticle colloids were prepared in a way similar to a published procedure.[30] The average diameter of particles is estimated to be 3 nm from the UV/visible absorption spectra.[30] The ZnO nanocrystalline thin films were prepared from the ZnO colloid by a procedure similar to that employed by Bedja et al.[22] Briefly, 100 mL of a 33 g/L colloid of ZnO nanoparticles in ethanol was applied onto a polished sapphire or CaF_2 window to form a thin film. The films were dried in air and then baked at 400 °C for 1 h. The film thickness was calculated to be about 2 μm on the basis of the volume and concentration of the ZnO colloid used to prepare the film and an approximate porosity of 50%.[31] When the films had cooled to 80 °C, they were placed into ethanolic solutions of Ru N3. Films with different amounts of adsorbed sensitizer molecules were obtained by controlling the time of sensitization and the concentration of the sensitizer from 1 hour in a 0.15 g/L solution (film (O. D.)$_{500\ nm}$ = 0.7) to 2 days in a 1.0 g/L solution (film (O. D.)$_{500\ nm}$ = 2.6). The sensitized film was washed with ethanol and dried in air. High purity Ru N3 was purchased from Solaronix (Lausanne, Switzerland).

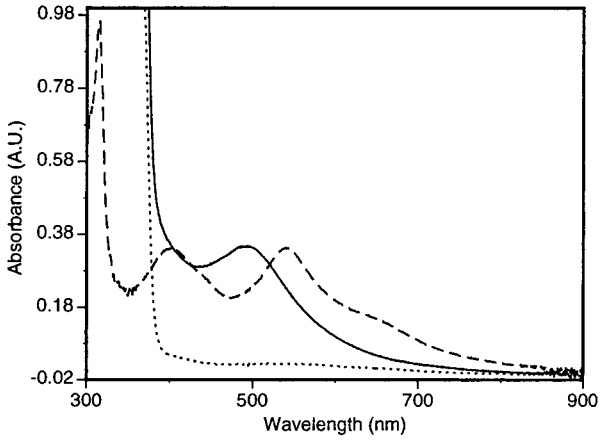

Figure 1. Comparison of UV/vis absorption spectra of Ru N3 on ZnO nanocrystalline film (solid line), Ru N3 in ethanol (dashed line), and naked ZnO nanocrystalline film (dotted line).

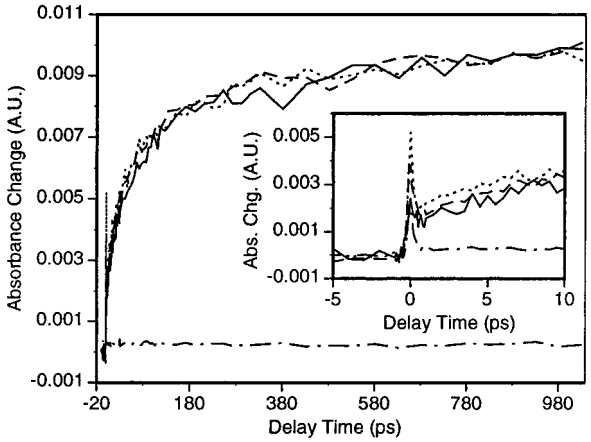

Figure 2. Injection kinetics of Ru N3 sensitized ZnO nanocrystalline film measured at 1900 cm^{-1} (solid line), 1950 cm^{-1} (dashed line), and 2000 cm^{-1} (dotted line). The lower, dotted dashed line is the response of the naked ZnO film under the same experimental conditions, scaled by a factor of 3 to match the spike around zero delay of the sensitized film signal. The inset is the same data shown on a shorter time scale.

Results

The UV−vis absorption spectrum of Ru N3 on ZnO nanocrystalline thin film is shown in Figure 1 (solid line). For comparison, the UV−vis spectra of Ru N3 in ethanol (dashed line) and the naked ZnO film (dotted line) are shown as well. The peak of the lowest MLCT transition of Ru N3 in ethanol is visible at 535 nm. In contrast, the peak of the lowest MLCT transition for Ru N3 on ZnO occurs around 500 nm. The naked film shows a slow increase in absorbance with decreasing wavelength from 900 to 400 nm, which is attributed to scattering of the nanocrystalline film. The absorbance onset at 370 nm of the naked film arises from the band gap transition.

Figure 2 shows the rise time of the mid-IR absorption measured at 1900, 1950, and 2000 cm^{-1} in a Ru N3 sensitized ZnO thin film after 400 nm excitation. The three traces are superimposable within the noise. There is also a small signal from the naked ZnO film under the same excitation power, as

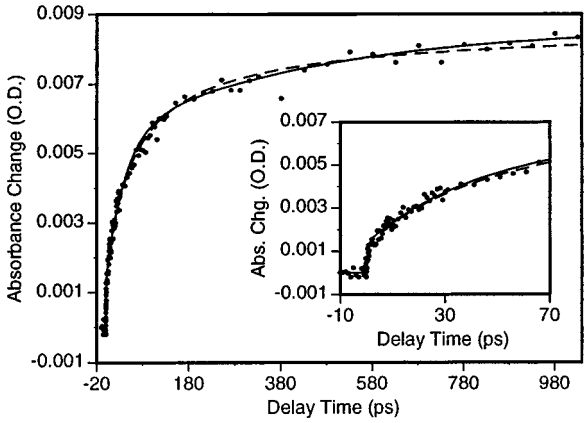

Figure 3. Injection kinetics of Ru N3 sensitized ZnO nanocrystalline film measured at 1900 cm-1 (filled circles) obtained by subtracting the naked ZnO film response. The solid line is a three exponential fit to the data and the dashed line is a fit of a model described in the text. The inset shows the same data on a shorter time scale.

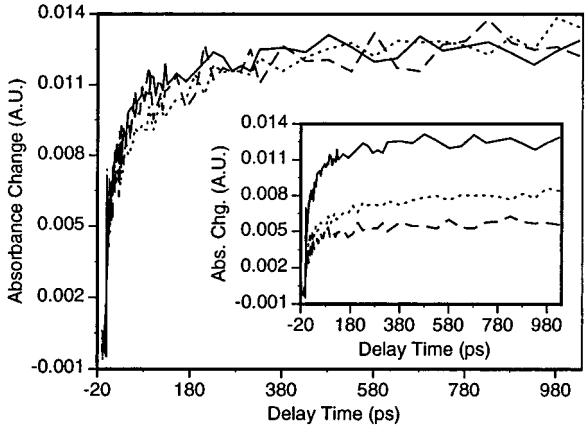

Figure 4. Comparison of injection kinetics of Ru N3 sensitized ZnO nanocrystalline films prepared with the following optical absorbances at 500 nm: 0.7 (solid line), 2.3 (dashed line), and 2.6 (dotted line). The data in the main panel have been scaled to the same final magnitude. The inset shows the same data without scaling.

shown by the dotted dashed line in Figure 2 which was measured at 1900 cm^{-1}. The signal from the naked film has been scaled down by a factor of 3 to match the fast spike at zero delay of the sensitized film, also measured at 1900 cm^{-1}. We believe the magnitude of the fast spike reflects the contribution of the naked ZnO film to the total signal from the sensitized film. To obtain the kinetics of electron injection, the scaled response of the naked film was subtracted from the signal from the sensitized film. Figure 3 shows a trace of the subtracted kinetics measured at 1900 cm^{-1} (filled circles). The solid line in Figure 3 is a three-exponential fit with the following time constants and amplitudes (in parentheses): subpicosecond rise (18%), a 42 ps rise (46%), and a 450 ps rise (36%). The exact time for the subpicosecond component could not be well characterized because of the subtraction of the spike at zero delay. The dashed line in Figure 3 is a fit to a model described later in the Discussion section.

Three nanocrystalline thin films were prepared with the following optical absorbance at 500 nm: 0.7, 2.3, and 2.6 O.D. Figure 4 shows traces of the rise of the electron signal in ZnO for the three films measured at 2000 cm^{-1} as the solid, dashed, and dotted traces, respectively, which have been scaled to the same final magnitude. The rise times of the signals for the three films are the same within the noise. The inset shows the original data for these films before scaling their amplitude.

Discussion

For Ru N3 sensitized TiO_2 nanoparticle thin film, a red shift was observed in the UV−vis absorption and photocurrent action spectrum compared to the absorption spectrum of the sensitizer in ethanol.[2] It was attributed to stabilization of the π^* orbital of the dcbpy ligand by delocalization into the orbitals of TiO_2 through the anchoring carboxyl groups.[2] This strong chelation of the surface is believed to contribute to the ultrafast electron injection measured in Ru N3 sensitized TiO_2 nanocrystalline thin films.[1,10,11] In contrast, the visible absorption spectrum of Ru N3 on ZnO is blue shifted relative to free Ru N3 in ethanol (see Figure 1). The reason for this blue shift is unclear.[21,22] However, the photocurrent action spectrum of a Ru N3 sensitized ZnO nanoparticle thin film, recently measured by Gratzel and co-workers,[21] closely resembled the absorption spectrum of the free dye in ethanol and did not show the blue shift of the absorption spectrum of the sensitized film. This result may indicate that only a fraction of the sensitizers on the ZnO surface contribute to the photocurrent action spectrum. The remainder of the sensitizers may have very low injection efficiency[21,22] which is believed to be strongly dependent on how the sensitizer binds to the surface.[5,6,21,22] The lack of red shift in the absorption may suggest the lack of strong mixing between the π^* orbital of the dcbpy ligand and accepting conduction band orbitals of ZnO.

As demonstrated previously in dye sensitized TiO_2 thin films,[3,8,9] we can measure the electron injection time in a Ru N3 sensitized ZnO film by measuring the rise of the mid-IR absorbance of injected electrons. To confirm the assignment of the mid-IR absorption to electrons in ZnO, we directly excited the band gap of ZnO at 267 nm and observed a broad featureless mid-IR absorption in the 1900 to 2000 cm^{-1} region. The signal appears instantaneously, consistent with instantaneous generation of charge carriers in ZnO. As shown in Figure 2, similar broad mid-IR absorption was observed in a Ru N3 sensitized ZnO film after excitation of the sensitizer MLCT band at 400 nm. The comparison with the naked ZnO film, as shown in Figure 2, suggests that the rise of the mid-IR signal contains only negligible contribution from the naked film. Thus, the mid-IR absorption signal observed for the sensitized films can be attributed to injected electrons.

The rise time of the mid-IR signal is a measurement of the electron injection kinetics from the Ru N3 dcbpy π^* orbital to ZnO, if there is negligible decay due to back electron recombination or electron relaxation on the same time scale. We assume negligible recombination on the <1 ns time scale, since back electron recombination in Ru N3 sensitized TiO_2 thin films occurs on the μs to ms time scale[10,20] As shown in Figure 2, the signal from the naked film shows negligible decay in the <1 ns time scale, indicating negligible cross-section decay due to electron relaxation. In contrast to the <100 fs injection time observed in Ru N3 sensitized TiO_2 thin films, the injection kinetics in the ZnO film are clearly much slower and non-single-exponential. As shown in Figure 3, the simplest multiexponential fit requires three components. Similar three-exponential kinetics were observed in all films studied, although the exact rise times varied slightly among different films. Unfortunately, our optical delay stage does not allow us to measure kinetics after 1 ns. As a result, we could not determine whether the injection process is complete within 1 ns. On the basis of the monotonic rise in the sensitized film signal even at 1 ns, it is possible that electron injection may continue well into the nanosecond time regime. In fact, Bedja and co-workers[22] recently measured the injection time of $[Ru(II)(bpy)_2(dcbpy)]^{2+}$ sensitized ZnO thin film in the

nanosecond time scale by microwave absorption and found a biphasic injection with lifetimes of 9.6 and 83 ns. Their measurement had a nanosecond time resolution and could not resolve the faster injection process observed in our study.

The observed multiexponential injection kinetics suggest that there exists a distribution of electron transfer rates between the Ru N3 molecules and ZnO nanoparticles in the film. This can result from a distribution of injection rates for sensitizer molecules in the first adsorbed layer as well as multilayer adsorption or aggregation. To study the effect of coverage level on injection, three Ru N3 sensitized ZnO films with different coverage were compared. As shown in the inset of Figure 4, the magnitude of the mid-IR signal at delay time <1 ns was inversely related to the surface coverage of the film as was the fast spike. Unfortunately, without the knowledge of the exact particle size in the film and the porosity, an estimate of the film thickness and layers of sensitizer coverage[7,32,31] is not very reliable. Thus, we cannot determine whether increasing coverage leads to the formation of aggregates, multilayer coverage, or both. They are all possible reasons for the observed reduced injection quantum yield on the <1 ns time scale in films with higher coverage. Since the injection kinetics are approximately the same for different films, we can conclude that the observed slow multiexponential injection dynamics result from an inhomogeneous distribution of injection rates for sensitizers in the first monolayer.

According to Marcus' theory for nonadiabatic electron transfer,[26] the observed multiexponential injection dynamics suggest that there is a distribution of electronic coupling, driving force, and/or density of states in ZnO. If we assume a Gaussian distribution, $g(V)$, of the population of sensitizers as a function of coupling matrix element, V, and use Marcus theory for nonadiabatic electron transfer rate, $k(V)$, we can solve a first-order kinetics equation to obtain an expression for the concentration of injected electrons, $N_e(t)$:

$$N_e(t) = 1 - \int_0^\infty g(V) e^{-k(V)t} dV \qquad (1)$$

$$g(V) = \frac{2\sqrt{\ln 2}}{\sqrt{\pi} D} \exp\left[-4 \ln 2 \left(\frac{V - V_0}{D}\right)^2\right] = \frac{2\sqrt{\ln 2}}{\sqrt{\pi} D} \exp\left[-4 \ln 2 \left(\frac{V}{D} - \frac{V_0}{D}\right)^2\right] \qquad (2)$$

$$k(V) = \frac{2\pi}{\hbar} V^2 \frac{1}{\sqrt{4\pi\lambda k_B T}} \exp\left[-\frac{(\Delta G_0 + \lambda)^2}{4\lambda k_B T}\right] = k(V_0) \frac{V^2}{V_0^2} = k(V_0) \frac{(V/D)^2}{(V_0/D)^2} \qquad (3)$$

where V_0 and $k(V_0)$ are the electronic coupling matrix element and rate at the peak of the Gaussian distribution, respectively; D the fwhm of the Gaussian distribution; ΔG^0 the driving force; and λ the reorganization energy. The kinetics $N_e(t)$, according to this model, depend on only two parameters: $k(V_0)$ and V_0/D. Satisfactory fits of the data can be obtained with unique values for these parameters. The best fit, shown by the dashed line in Figure 3, yields $1/k_0 = 133$ ps and $V_0/D = 0.45$. Although this model fits the data pretty well, other factors should also be considered. The Marcus equation used above may need to be modified to take into account the density of accepting states in the semiconductor, which is a size-dependent property for quantum-confined systems. The radius of ZnO at which quantum confinement begins has been estimated to be about 5 nm,[27,28] although radii as small as 3[29] and as large as 7[30] or 10 nm[33,34] have been estimated. The radius for the colloidal nanoparticles used to prepare the films is about 1.5 nm, and these particles show quantum confinement effects in the blue-shifted exciton band. However, in the sintering process during film preparation, the particles may partially fuse together forming larger particles. As a result, there may be a distribution of effective particle sizes in the film and corresponding distributions of energy levels and density of states for the electrons as a result of quantum confinement. This will also lead to a distribution of electron injection rates. While the effect of quantum confinement on electron transfer rate in nanoparticles is an important property that has yet to be demonstrated, the thin film samples studied are not an ideal system to address this problem because of the ill defined size distribution. We are now investigating this effect in sensitized colloidal ZnO particles that have well controlled and readily adjustable size.

The observed multiexponential injection dynamics in ZnO is very different from the <100 fs injection dynamics for the same sensitizer on TiO_2 thin films.[3,8−12] Multiexponential electron injection dynamics were also observed in a series of coumarin dye sensitized ZnO nanoparticle colloids in methanol by Murakoshi and co-workers.[35] They recently measured the electron injection time by the fluorescence lifetime of the dyes with femtosecond time resolution and observed multiexponential injection kinetics with lifetimes from hundreds of femtoseconds to nanoseconds. Interestingly, the injection time of coumarin 343 (C343) sensitized TiO_2 colloidal nanoparticles in aqueous solutions has been found to be about 150 fs.[24,36] Murakoshi and co-workers[35] suggested that the dramatic difference in the injection rate of C343/TiO2 in aqueous solution and C343/ZnO in methanolic solution may be caused by the difference in solvent.

Since both the Ru N3 sensitized TiO_2 and ZnO samples are dry films, the observed different electron injection kinetics in these systems cannot be attributed to the difference in solvents. We would like to suggest that they may be caused by the difference in electronic coupling between the Ru N3 dcbpy π^* orbital and the accepting orbitals in TiO_2 and ZnO and/or their density of states. Assuming an effective mass of 5.6 m_e and 0.24 m_e for the conduction band electrons in TiO_2 and ZnO thin films, respectively, the density of states in the conduction band of ZnO was estimated to be 113 times smaller than that in TiO_2.[37] This alone would contribute to 100 times slower electron injection time in ZnO. However, differences in the density of states can only be considered as an estimate because of the uncertainty in the value of the electron effective mass in TiO_2 films. Furthermore, the quantum confinement effect in ZnO would change the accepting state from a continuous band to more discrete energy levels. The effect of quantum confinement on the injection time has yet to be investigated, but the decrease in the density of states might further slow the electron injection kinetics. Also, the exact nature of the accepting state in these two films is still unclear. For TiO_2, the role of localized surface states associated with Ti^{4+} in the interfacial charge transfer process remains to be resolved.[25] Another main difference in these two semiconductor materials is that the states near the conduction band edge of ZnO consist of the 4s orbitals of Zn^{2+},[38] while those of TiO_2 consist of the 3d orbitals of Ti^{4+}.[1,39] It is reasonable to expect significant difference in their coupling with the π^* orbital of the dcbpy ligand, although the quantitative difference has yet to be determined. We are trying to resolve this issue using electronic structure calculations.

Conclusion

In conclusion, we have measured the injection time of a Ru N3 sensitized ZnO nanocrystalline thin film and found the kinetics to be highly nonexponential. A three-exponential fit to the data shows three components consisting of a subpicosecond rise (18%), a 42 ps rise (46%), and a 450 ps rise (36%). The rise time of the absorption was the same across a 100 cm^{-1} region from 2000 to 1900 cm^{-1}. For films with different sensitizer coverage, the amplitude of electron absorption signal at 1 ns is smaller in films with higher sensitizer coverage, while the injection kinetics are the same for delay times < 1 ns. The nonexponential injection kinetics suggest that even with less than one monolayer of sensitizers, there exists a distribution of electron transfer rates for different sensitizer molecules. The nonexponential injection kinetics can be satisfactorily fit by a model that assumes a Gaussian distribution of electronic coupling between the π^* orbital of the Ru N3 dcbpy ligand and the accepting orbital in ZnO, but effects due to distribution of driving force and density of states in ZnO caused by quantum confinement may also need to be considered.

These injection dynamics on ZnO are much slower than those for the same sensitizer on TiO_2, indicating differences in the electronic coupling with the surfaces and differences in the density of acceptor states in these semiconductors. This slower nonadiabatic electron transfer process provides an opportunity to examine the dependence of interfacial ET rates on various parameters such as solvent reorganization energy, driving force, coupling matrix element, and density of states in the semiconductor. Work toward this systematic examination of interfacial ET theory is ongoing.

Acknowledgment. We are grateful to the financial support by the Chemical Science Division, U.S. Department of Energy (Grant # DE-FG02-98ER14918). This work is also supported in part by the Petroleum Research Fund, administered by the American Chemical Society.

References and Notes

(1) Hagfeldt, A.; Gratzel, M. *Chem. Rev.* **1995**, *95*, 49−68.
(2) Nazeeruddin, M. K.; Kay, A.; Rodicio, I.; Humphrybaker, R.; Muller, E.; Liska, P.; Vlachopoulos, N.; Gratzel, M. *J. Am. Chem. Soc.* **1993**, *115*, 6382−6390.
(3) Asbury, J. B.; Ellingson, R. J.; Ghosh, H. N.; Ferrere, S.; Nozik, A. J.; Lian, T. *J. Phys. Chem. B* **1999**, *103*, 3110−3119.
(4) Grunwald, R.; Tributsch, H. *J. Phys. Chem. B* **1997**, *101*, 2564−2575.
(5) Argazzi, R.; Bignozzi, C. A.; Heimer, T. A.; Castellano, F. N.; Meyer, G. J. *Inorg. Chem.* **1994**, *33*, 5741−5749.
(6) Murakoshi, K.; Kano, G.; Wada, Y.; Yanagida, S.; Miyazaki, H.; Matsumoto, M.; Murasawa, S. *J. Electroanal. Chem.* **1995**, *396*, 27.
(7) Shklover, V.; Haibach, T.; Bolliger, B.; Hochstrasser, M.; Erbudak, M.; Nissen, H. U.; Zakeeruddin, S. M.; Nazeeruddin, M. K.; Gratzel, M. *J. Solid State Chem.* **1997**, *132*, 60−72.
(8) Asbury, J. B.; Ghosh, H. N.; Ellingson, R. J.; Ferrere, S.; Nozik, A. J.; Lian, T. Femtosecond IR Study of Ru Dye Sensitized Nanocrystalline TiO_2 Thin Films: Ultrafast Electron Injection and Relaxation Dynamics in *Ultrafast Phenomena XI*, 1998.
(9) Ellingson, R. J.; Asbury, J. B.; Ferrere, S.; Ghosh, H. N.; Lian, T.; Nozik, A. J. *J. Phys. Chem. B* **1998**, *102*, 6455.
(10) Tachibana, Y.; Moser, J. E.; Gratzel, M.; Klug, D. R.; Durrant, J. R. *J. Phys. Chem.* **1996**, *100*, 20056−20062.
(11) Hannappel, T.; Burfeindt, B.; Storck, W.; Willig, F. *J. Phys. Chem. B* **1997**, *101*, 6799−6802.
(12) Heimer, T.; Heilweil, E. J. *J. Phys. Chem. B* **1997**, *101*, 10990−10993.
(13) Enright, B.; Fitzmaurice, D. *J. Phys. Chem.* **1996**, *100*, 1027.
(14) O'Regan, B.; Gratzel, M.; Fitzmaurice, D. *J. Phys. Chem.* **1991**, *95*, 10525−10528.
(15) Rothenberger, G.; Fitzmaurice, D.; Gratzel, M. *J. Phys. Chem.* **1992**, *96*, 5983.
(16) Doherty, S.; Fitzmaurice, D. *J. Phys. Chem.* **1996**, *100*, 10732−10738.
(17) Solbrand, A.; Henningsson, A.; Sodergren, S.; Lindstrom, H.; Hagfeldt, A.; Lindquist, S.-E. *J. Phys. Chem. B* **1999**, *103*, 1078−1083.
(18) Solbrand, A.; Lindstrom, H.; Rensmo, H.; Hagfeldt, A.; Lindquist, S.-E. *J. Phys. Chem. B* **1997**, *101*, 2514.
(19) Hagfeldt, A.; Bjorksten, U.; Gratzel, M. *J. Phys. Chem.* **1996**, *100*, 8045−8048.
(20) Haque, S. A.; Tachibana, Y.; Klug, D. R.; Durrant, J. R. *J. Phys. Chem. B.* **1998**, *102*, 1745−1749.
(21) Redmond, G.; Fitzmaurice, D.; Gratzel, M. *Chem. Mater.* **1994**, *6*, 686−691.
(22) Bedja, I.; Kamat, P. V.; Hua, X.; Lappin, A. G.; Hotchandani, S. *Langmuir* **1997**, *13*, 2398−2403.
(23) Rensmo, H.; Keis, K.; Lindstrom, H.; Sodergren, S.; Solbrand, A.; Hagfeldt, A.; Lindquist, S.-E.; Wang, L. N.; Muhammed, M. *J. Phys. Chem.* **1997**, *101*, 2598−2601.
(24) Ghosh, H. N.; Asbury, J. B.; Lian, T. *J. Phys. Chem. B* **1998**, *102*, 6482−6486.
(25) Ghosh, H. N.; Asbury, J. B.; Weng, Y.; Lian, T. *J. Phys. Chem. B* **1998**, *102*, 10208−10215.
(26) Miller, R. J. D.; McLendon, G. L.; Nozik, A. J.; Schmickler, W.; Willig, F. *Surface electron transfer processes*; VCH Publishers, Inc., New York, 1995.
(27) Haase, M.; Weller, H.; Henglein, A. *J. Phys. Chem.* **1988**, *92*, 482−487.
(28) Weller, H. *Adv. Mater.* **1993**, *5*, 88−95.
(29) Wong, E.; Bonevich, J.; Searson, P. *J. Phys. Chem. B* **1998**, *102*, 7770−7775.
(30) Meulenkamp, E. *J. Phys. Chem. B* **1998**, *102*, 5566−5572.
(31) Hoyle, R.; Sotomayor, J.; Will, G.; Fitzmaurice, D. *J. Phys. Chem. B* **1997**, *101*, 10791−10800.
(32) O'Regan, B.; Moser, J.; Anderson, M.; Gratzel, M. *J. Phys. Chem.* **1990**, *94*, 8720−8726.
(33) Brus, L. *J. Phys. Chem.* **1986**, *90*, 2555−2560.
(34) Brus, L. *J. Chem. Phys.* **1983**, *79*, 5566−5571.
(35) Murakoshi, K.; Yanagida, S.; Capel, M.; Castner, J. E. W. *Interfacial Electron Transfer Dynamics of Photosensitized Zinc Oxide Nanoclusters*; ACS Symposium Series 679, The American Chemical Society: Washington, DC, 1997.
(36) Rehm, J. M.; McLendon, G. L.; Nagasawa, Y.; Yoshihara, K.; Moser, J.; Gratzel, M. *J. Phys. Chem.* **1996**, *100*, 9577−9578.
(37) Redmond, G.; O'Keefe, A.; Burgess, C.; MacHale, C.; Fitzmaurice, D. *J. Phys. Chem.* **1993**, *97*, 11081−11086.
(38) Henrich, V.; Cox, P. *The Surface Science of Metal Oxides*; Cambridge University Press: Cambridge, 1996.
(39) Sorantin, P.; Schwartz, K. *Inorg. Chem.* **1992**, *31*, 567−576.